International Journal of Biological Macromolecules 87 (2016) 366–374

Contents lists available at ScienceDirect

International Journal of Biological Macromolecules

journal homepage: www.elsevier.com/locate/ijbiomac

Novel guar gum/Al_2O_3 nanocomposite as an effective photocatalyst for the degradation of malachite green dye

Deepak Pathania [a], Rishu Katwal [a], Gaurav Sharma [a,*], Mu. Naushad [b,*], Mohammad Rizwan Khan [b], Ala'a H. Al-Muhtaseb [c]

[a] School of Chemistry, Shoolini University, Solan, 173212 Himachal Pradesh, India
[b] Department of Chemistry, College of Science, Building #5, King Saud University, Riyadh, Saudi Arabia
[c] Department of Petroleum and Chemical Engineering, Faculty of Engineering, Sultan Qaboos University, Muscat, Oman

ARTICLE INFO

Article history:
Received 17 December 2015
Received in revised form 25 February 2016
Accepted 28 February 2016
Available online 2 March 2016

Keywords:
Nanocomposite
Dyes
Photodegradation
Antibacterial activity

ABSTRACT

Guar gum/Al_2O_3 (GG/AO) nanocomposite was prepared using simple and cost effective sol–gel method. This nanocomposite was characterized by several analytical techniques viz. scanning electron microscopy (SEM), transmission electron microscopy (TEM), X-ray diffraction (XRD), thermal analysis (TGA/DTA), Fourier transform infrared spectroscopy (FTIR) and ultraviolet-visible spectroscopy (UV–vis). The FTIR analysis confirmed that GG/AO composite material was formed. TEM images inferred the particle size in the range between 20 and 45 nm. GG/AO nanocomposite exhibited good photocatalytic performance for malachite green (MG) dye (dye initial concentration 1.5×10^{-5} M) degradation from aqueous phase. The adsorption followed by photocatalysis and coupled adsorption/photocatalysis reaction achieved about 80% and 90% degradation of MG dye under solar irradiation. Antibacterial test showed the excellent activity of GG/AO nanocomposite against *Staphylococcus aureus*.

1. Introduction

Population explosion, extensive industrialization and advancement in agricultural techniques have results in the degradation of aquatic environment due to the discharge of non-degradable and hazardous materials into the aquatic system [1–3]. Textile industry which is one of the most important water consumers produces highly colored and complex wastewater [4]. More than 100,000 commercially obtain dyes with over 7.105 t of dyestuff produce yearly. Dyes include a broad spectrum of different chemical structures [5,6]. The discharge of dye-containing effluents into the water bodies is undesirable as the dyes breakdown to toxic, carcinogenic and mutagenic products [7,8]. These dyes can remain in the waste water for a long time. It cannot be used for reuse purposes without further treatment. There are several techniques which are common for dye removal viz. chemical oxidation, coagulation, microbial degradation, photocatalysis and adsorption. Recently, adsorption and heterogeneous photocatalytic degradation of organic molecules is the most effective and economic process for solving the toxic environmental impact of hazardous wastes and toxic pollutants in aqueous medium [9–11]. The main advantage of adsorption and photocatalytic degradation for the control of water pollution are less investment in terms of initial development cost, easy operation, simple and recovery of the adsorbent material [12]. The photocatalytic process leads to oxidation–reduction and offers superior solution for decolonization, breakdown of dye. Therefore, the mineralization efficiency would be controlled by both adsorption and photoactivity of photocatalyst.

Malachite green (MG) dye is environmentally insistent and highly toxic to a wide range of aquatic as well as terrestrial animals. It causes several severe public health threats and also poses potential environmental complications. MG is a basic dye which is extensively used in industries for dyeing silk, leather, cotton, hair color, wool and paper. It has also been used to controls protozoan infection and other disease caused by helminthes on aquatic organism. MG is highly cytotoxic to mammalian cell and carcinogenic to liver, thyroid and other organs of animals [13,14]. It causes the damage to liver, growth and fertility rates, kidney, heart, eyes, lungs, and produces teratogenic effects in rats and mice [15]. Due to diverse problems due to various dyes, there has been a strong interest in the inorganic–polymer composite for the environmental remediation.

Nowadays, metal oxide/polymer nanocomposites have gained much consideration due to their potential to offer the coupled features of polymeric materials with those of inorganic materi-

* Corresponding authors.
E-mail addresses: gaurav8777@gmail.com (G. Sharma), shad123@gmail.com (Mu. Naushad).

http://dx.doi.org/10.1016/j.ijbiomac.2016.02.073
0141-8130/

als. Biopolymers act as surface capping agents when the metal oxide nanoparticles are embedded or encapsulated in them. The advantages of biopolymer include easy availability, renewability, biodegradability, nontoxicity, low cost, low specific gravity, high toughness, acceptable specific strength, and enhanced energy recovery [16].

Guar gum is a polysaccharide made up of $(1\rightarrow4)-\beta$-D mannopyranosyl linear chains units attached by $(1\rightarrow6)$ linkages of α-D-galactopyranose [17]. It used in food nutrition, biotechnology, materials science, drugs, pharmaceuticals, agriculture, environmental protection, and recently in gene therapy [18,19]. Guar gum based material has synergetic effect from biopolymers and inorganic materials. They have been used as catalyst [20], solar cells [21], low-temperature NO_2 sensors [22], tissue engineering [23], drug delivery [24], adsorbent [25], molecular recognition system etc. Literature survey revealed that only few studies have been reported on the guar gum based nanocomposite materials [26–28].

Among various inorganic nanoparticles, Al_2O_3 has attracted interest due to its applicability in different fields such as fire retard, catalyst, surface protective coating, and composite materials [29,30]. Al_2O_3 is an electrical insulator having high thermal conductivity. Aluminum oxide based nanocomposites such as aluminum oxide/polyacrylamide-based cryogels [31,32], aluminum/aluminum oxide nanocomposites [33] and poly(ether-ether-ketone) aluminum oxide [34] have been synthesized.

The development of antimicrobial agent is an important impact on natural environment. Microbial contamination and growth are potential risk for human health. To prevent the microbe attack on textiles, spread of disease, injury-induced infection, stains on textile materials and deterioration of textiles caused by fungus and bacteria, the demand of different antimicrobial agents suitable for textile application on the market has been increased dramatically [35]. To treat organic pollutants and microbial containing wastewater, the researches have recently been focused on advanced nano materials.

The present work focuses on the removal of MG form aqueous phase using both adsorption and photocatalysis phenomenon. To the best of our information, no study has been reported on the fabrication of GG/AO nanocomposite with photocatalytic activity and antimicrobial activity. The sun light activity of GG/AO nanocomposite will be exploited for the removal MG through coupled adsorption and photocatalysis processes. The antimicrobial activity of GG/AO nanocomposite was evaluated against *Staphylococcus aureus*.

2. Experimental

The chemicals such as guar gum, MG dye, sodium nitrate and acetonitrile used in this study were purchased from CDH Pvt. Ltd., India. All the solutions and dilution were made in double distilled water.

2.1. Preparation of aluminum oxide nanoparticles (AO NPs)

The AO NPs were prepared electrochemically using a simple two-electrode cell in aqueous solution containing water: acetonitrile solvent 200 mL (12:1) and sodium nitrate supporting electrolyte (1.25 mM). The sacrificial aluminum plate ($2\times5\,cm^2$) and inert platinum ($1\times1\,cm^2$) were utilized as a sacrificial anode and cathode, respectively. Before the electrolysis, both electrodes were cleaned with hydrochloric acid and double distilled water. The distance between both the electrodes was fixed at 1 cm for all the experiments. The electrolysis reaction was performed at 100 mA current for 2 h with constant stirring at room temperature. After the electrolysis, white precipitates were centrifuged, washed with ethanol and double distilled water several times. The product was then dried at 60 °C in a hot air oven for 2 h. The material obtained was calcined at 1200 °C for 1 h.

2.2. Preparation of GG/AO nanocomposite

GG/AO nanocomposite has been prepared by simple and ambient sol-gel method. In typical synthesis procedure, 150 mg of guar gum was dissolved in 50 mL deionized water and stirred for 2 h at 50 °C. The suspension of AO NPs was added into above solution with continuous shaking and followed by the addition of potassium persulphate solution drop wise. The resultant mixture was stirred for 3 h on magnetic stirrer at 50 °C. The white colored precipitates obtained were then kept for digestion for 24 h. The supernatant liquid was decanted and the gels were filter under suction and washed with distilled water to eliminate the extra impurities. The material thus obtained was dried in an hot air oven at 50 °C.

2.3. Adsorption and photocatalytic studies

The adsorption and photocatalytic efficiency of GG/AO nanocomposite was performed for MG dye degradation. For this, 100 mg of GG/AO composite was added into 1.5×10^{-5} M solution of MG dye to form suspension [36,37]. The adsorption and photocatalytic studies were executed using a pyrex glass beaker and magnetic stirred for controlled agitation. During adsorption experiments, the suspension was retained in dark to adsorption and desorption of MG dye molecule. As the equilibrium was achieved, the suspension was exposed to sunlight with intermittent agitation for further photocatalysis. Prior to photocatalysis, suspension of dye and composite was stirred continuously and exposed to sunlight directly. Both the reaction set was compared to study the effect of the conditions. During the reaction, 5 mL solution was withdrawn at different time intervals and centrifuged. The photocatalytic degradation of the MG dye was investigated at 620 nm. The degradation percentage of dye was calculated using formula as:

$$\%\text{Degradation} = \frac{C_e - C_t}{C_e}\times100$$

where C_e and C_t are the concentrations of dye at equilibrium and at time t.

The rate of photodegradation of dye fitted pseudo-first-order kinetic model as follow [38,39].

$$\ln\frac{A_o}{A_t} = k_{app}t$$

where A_o is the concentrations of dye before illumination, A_t is the concentration of dye at time t and k_{app} is the apparent rate constant.

2.4. Antimicrobial activity of GG/AO nanocomposite

Antimicrobial activity of GG/AO nanocomposite was evaluated as per method described earlier with some modifications [40,41]. In this method, three tubes of bacterial suspension 5 mL (with a concentration of 10^7 CFU/mL of *S. aureus*) cultured in NB were prepared. Out of three tubes of bacterial suspension, two were supplemented with different amounts of GG/AO nanocomposite (0.4 μg/mL and 0.8 μg/mL). A 100 μL sample of bacterial suspension from each tube was then plated in three different nutrient agar plates. Nanoparticle free bacterial suspension incubated under the same conditions was used as controls. The plates were then incubated at 37 °C. The tubes of bacterial suspension were incubated at 37 °C on a rotary shaker at 200 rpm for 24 h. The numbers of resultant colonies of *S. aureus* were counted after 24 h of incubation.

X-ray diffraction analysis (XRD) (X-ray Diffractometer Panalytical.s X.Pert Pro) of the nanocomposite material was recorded using Cu Ka radiation (k = 1.5418 Å). SEM (S-3400N, Hitachi, Japan) image of GG/AO nanocomposite were recorded at different magnifications. Transmission electron microscopy studies (FEI Tecnai F 20), of GG/AO nanocomposite was determined by placing a drop of suspensions of GG/AO nanocomposite prepared in ethanol onto a carbon copper grid. The UV–vis spectra (Systronics 2202 spectrophotometer) of GG/AO nanocomposite were recorded in distilled water. The spectrum showed featureless absorption in the 200–600 nm regions. The band gap energy was determined using the Tauc relation. Fourier transforms infra-red spectra (Model RZX; Perkin Elmer) of GG/AO nanocomposite were taken by KBr disc method. Thermogravimetric and differential thermal analysis were performed on thermal analyzer (Perkin Elmer, model). Sample weight varied from 10 to 15 mg and heated from up to 600 °C at a heating rate of 15 °C min^{-1} in nitrogen atmosphere.

3. Results and discussion

3.1. Structure analysis and morphology of AO NPs and GG/AO nanocomposite

The XRD pattern of GG/AO nanocomposite is shown in Fig. 1. The XRD result showed the amorphous nature of nanocomposites. The XRD exhibited characterization peaks of aluminum oxide (AO) at scattering angles (2θ) of 35.5°, 32.9°, 38.1°, 61.3°, 67.1°. All the peaks of AO were from JCPDS No. 46-1212 standard file [42]. The broadening of peaks indicated the formation of GG/AO nanocomposite. Fig. 2(a, b) illustrates the SEM images of guar gum and GG/AO nanocomposite. The guar gum showed bean shape morphology. The SEM micrograph of GG/AO showed the agglomeration of particles and formation of the nanocomposite. TEM micrograph of AO NPs and GG/AO nanocomposite is shown in Fig. 3(a, b). The TEM observation confirmed the average diameter of nanoparticles in the range of 20–35 nm. TEM micrographs inferred the dispersed homogeneous particles with diameters between 20–45 nm. The light part guar gum wrapped dark part of AO NPs. Fig. 4 shows the UV–vis spectra of GG/AO nanocomposite. The absorption bands at about 210 nm were attributed due to AO NPs and 240 nm for GG/AO nanocomposite [43,44]. The absorption peak of GG/AO nanocomposite showed evident red-shift phenomenon, showing strong interactions between polymer matrix and AO NPs. The shifting of the absorption bands was due to the interaction between a polymer matrix and nanoparticles [42]. The band gap of composite was calculated using Tauc Relation [45].

$$\alpha h\nu = \beta\left(h\nu - E_g\right) n$$

where α = absorption coefficient = 2.303 A/l, E_g = optical band gap, $h\nu$ is the photon energy, β = band tailing parameter, and n = ½ for direct band gap. The optical band gap was determined by extrapolating the straight portion of curve between $(\alpha h\nu)^2$ and $h\nu$ when, α = 0. The band gap as calculated from Tauc plot was found to be 3.02 eV.

FTIR analysis of GG and GG/AO nanocomposite is shown in Fig. 5. For GG spectra, the peaks at 3600–3400 cm^{-1} were assigned to O—H stretching vibrations of water molecule. The absorbance peaks at 2927 cm^{-1} and 1445 cm^{-1} corresponds to C—H stretching and C—O—C asymmetric bending [28]. The peaks at 1155 cm^{-1}, 1023 cm^{-1} and 1676 cm^{-1} might be due to C—O—C stretching, hydroxylic C—O single band stretching of C—O—C group in the anhydroglucose ring and ring stretching of galactose and mannose band, respectively [46]. The change in the intensity of some functional groups and appearance of new peaks in the GG/AO spectrum also confirmed the formation of nanocomposite. The sharp peaks at 533 cm^{-1}, 553 cm^{-1} corresponded to Al—O—Al bending mode. A weak peak at 821 cm^{-1} was due to Al—O stretching vibration [47].

3.2. Thermogravimetric analysis

Thermogravimetric curves of GG, AO and GG/AO nanocomposite is shown in Fig. 6. The total weight loss between the temperatures 90–520 °C was found to be 91.5%. It is evident from Fig. 6(a) that 3.7% weight loss was observed up to 100 °C which might be due to the removal of water molecule. Thermal degradation of GG was completed in two steps, 251–308 °C and 308–518 °C [48]. Initial decomposition temperature (IDT) was 251 °C while, final decomposition temperature (FDT) was 308 °C. In DTA studies, GG has been exhibit one exothermic peak at 291 °C corresponded to 251–308 °C in TGA.

In case of AO NPs, the total weight loss at the temperature of 100–600 °C was found to be 7.4%. The weight loss at temperature 32 °C was 0.3% only due to the removal of water molecule. The initial decomposition temperature was 93 °C and final decomposition temperature was 341 °C. It might be due to the easily adsorbed water which can exist stably to a certain temperature [49]. DTA studies of AO NPs revealed only one exothermic peak at 58 °C which was due to the decomposition stage in TGA at 93–341 °C (Fig. 6(b).

In case of GG/AO nanocomposite, the total weight loss at the temperature of 30–585 °C was found to be 11.8%. The decomposition of nanocomposite occurred in three stages. In the first stage, degradation occurred at 100 °C with 5.8% weight loss, which confirmed the loss of hydrogen bonded water molecule present at the surface, second stage was between 200 to 310 °C and the third decomposition was between 310 to 517 °C with the weight loss 4.6 and 1.4%, respectively which might be due to the degradation of organic part (Fig. 6(c). After 517 °C, very low weight loss was observed. Thus, it is evident from the TGA data that GG/AO nanocomposite was thermally more stable than the raw material. In DTA studies of GG/AO nanocomposite, three exothermic peaks at 47 °C, 290 °C and 502 °C assigned to the decomposition stage between 31–100 °C, 200–310 °C and 310–517 °C, respectively in TGA.

3.3. Photodegradation of dye

Photocatalysis of GG/AO nanocomposite was studied at different processes such as adsorption in dark followed by photocatalysis and coupled adsorption/photocatalysis under sunlight irradiation as shown in Fig. 7.

For the adsorption followed by photocatalysis process, the MG dye solution containing GG/AO nanocomposite was kept in dark to establish adsorption/desorption equilibrium. For further photodegradation process, the solution was exposed to sunlight to absorb free dye which is present in the solution. The decrease in the absorption band intensities in the presences of nanocomposite with irradiation time was observed for MG clearly revealed that the dye was degraded effectively by nanocomposite (Fig. 7(a). It was observed that only 41% MG dye was adsorbed by GG/AO under dark conditions and 81% of MG Dye degraded in sunlight (Fig. 7(c). It might be possible that the surface of photocatalyst was covered by dye molecules and degradation was suppressed. But when solution was irradiated under sun light, electron hole pair was generated, which reacted with water to release hydroxyl and super oxide radical [50]. The super oxides break the conjugation of molecules. Adsorption followed by photocatalysis, the mechanism was earlier reported by our research group [25]. The photo degradation of MG dye using GG/AO nanocomposite plot of ln A_o/A_t vs irradiation time showed a linear correlation (Fig. 7(e). Thus adsorption followed by photocatalysis of MG dyes was fit-

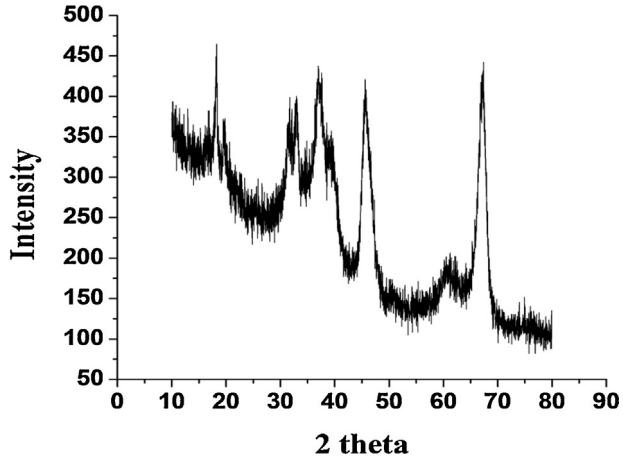

Fig. 1. XRD pattern of GG/AO nanocomposite.

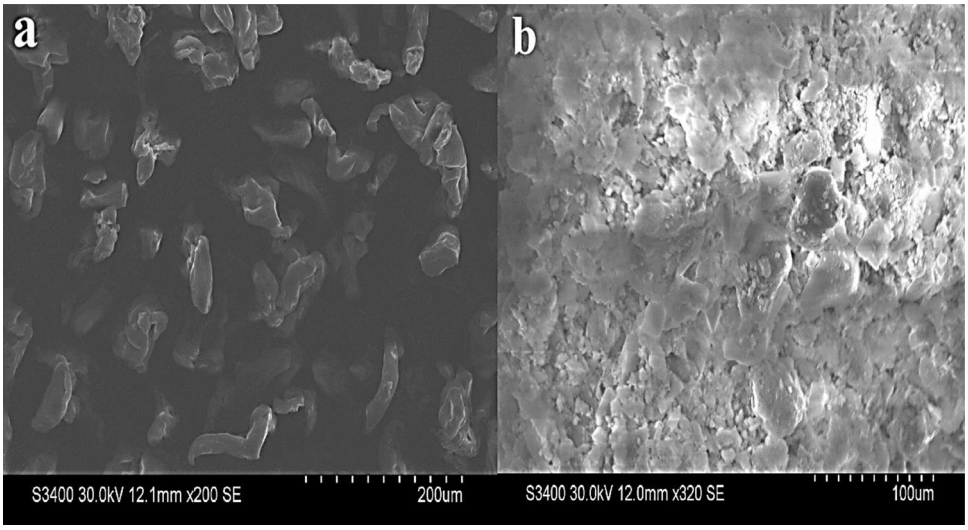

Fig. 2. SEM micrograph of (a) GG (b) GG/AO nanocomposite.

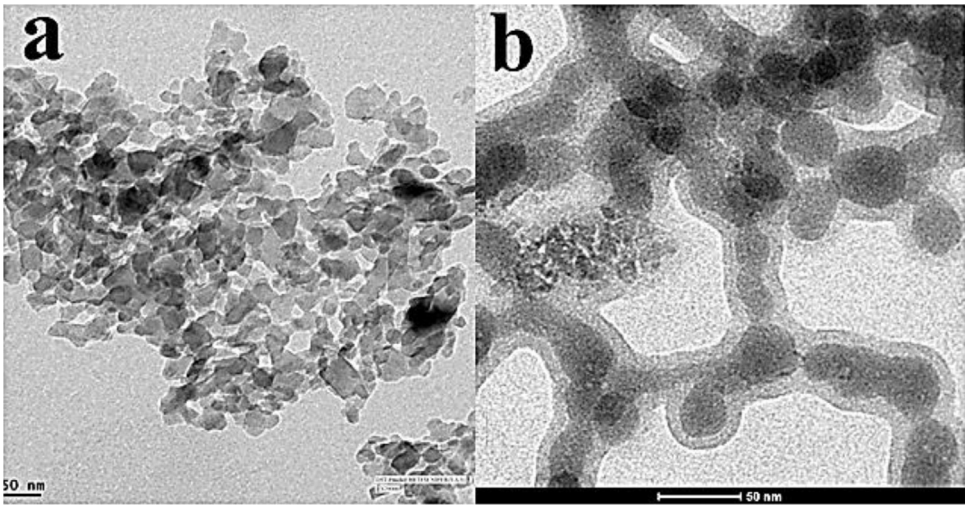

Fig. 3. TEM micrographs of GG/AO nanocomposite.

Table 1
% Removal of MG by GG/Al_2O_3 nanocomposite under sunlight, rate constants and linear coefficients from log C_0/C_t vs T plots.

Dye	Concentration	Adsorption followed by photocatalysis synergetic effect of adsorption/photocatalysis						
		% degradation in dark	% degradation in light	k_{app} (min^{-1})	R^2	% removal of dye in light	kapp (min-1)	R^2
MG	1.5×10^{-5}	41	81	−0.06679	0.95122	90	0.01893	0.95082

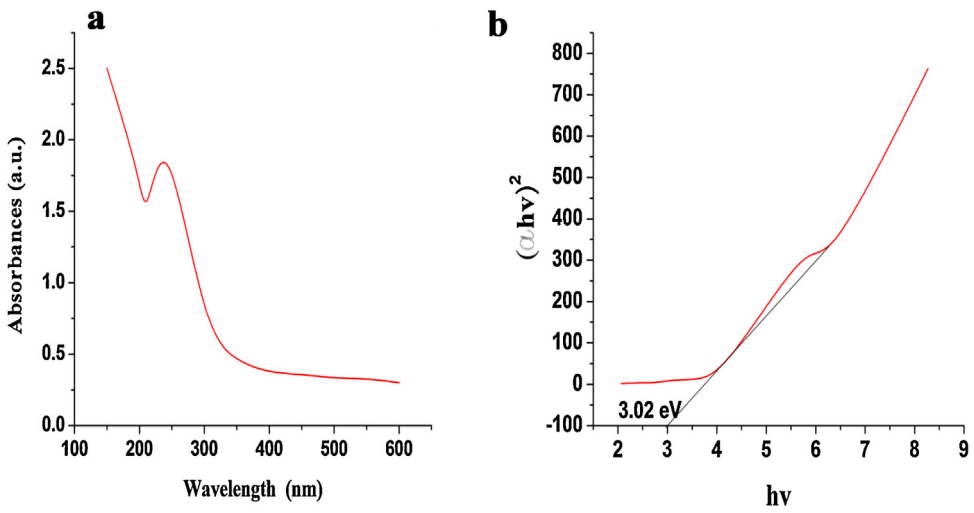

Fig. 4. UV–vis spectra of (a) GG/AO nanocomposite and(b) Plot of $(\alpha h\nu)^2$ vs $h\nu$.

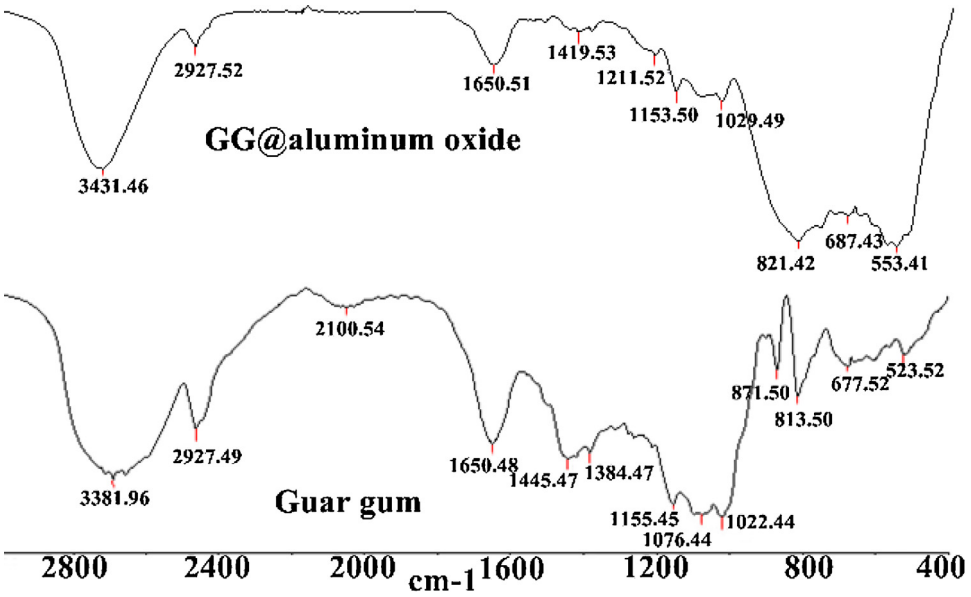

Fig. 5. FTIR spectra of GG and GG/AO nanocomposite.

ted to pseudo-first-order kinetics [50]. The rate constant k for MG dye and the value of correlation coefficient (R^2) for MG is shown in Table 1. The coupled adsorption/photocatalysis process directly in sunlight involves the adsorption of dye onto the material and photodegradation of dyes molecules at the same time. UV–vis spectral changes of MG in coupled adsorption/photocatalysis are shown in Fig. 7(b). The photocatalytic degradation percentage of MG dyes by GG/AO nanocomposite was found to be 90% in 220 min of photo irradiation as shown in Fig. 7(d). This study indicated the higher removal of dye was achieved as compared to adsorption followed by photocatalysis. In coupled process, we assumed simultaneous adsorption of dyes onto the photocatalyst surface and generation of electron-hole pairs on absorption of light at same time and generate free radicals to disrupt the conjugation in the adsorbed and free dye molecules present in the solution and hence degrade the dye [51]. The degraded dye products left the surface of nanocomposite free for further adsorption and photocatalysis. The dye adsorption onto the adsorbent can facilitate the photodegradation process and increases the degradation rate and reduces the degradation time [25]. The proposed mechanism for the coupled adsorption/photocatalysis degradation of MG dye is shown as follows:

$$GG/AO + MGDye \rightarrow GG/AO{-}Dyeadsorbed(Sunlight)$$

$$GG/AO(h^+)\text{-}Dyeadsorbed + H_2O \rightarrow GG/AO(OH^\bullet)\text{-}Dye + H^+$$

$$GG/AO(h^+){-}Dyeadsorbed + OH^- \rightarrow GG/AO(OH^\bullet)\text{-}Dye$$

$$GG/AO(e^-){-}Dyeadsorbed + O_2 \rightarrow GG/AO(O_2{}^\bullet)\text{-}Dye$$

$$O_2{}^{-\bullet} \text{ or } OH^\bullet + \text{Dye-GG/AO} \rightarrow \text{Intermediate Product} \rightarrow \text{Degraded Product} + \text{Free GG/AO for reuse}$$

Thus photodegradation was better in coupled adsorption/photocatalysis condition. The kinetics of MG dye degradation showed a linear correlation in Fig. 7(f). Thus, coupled adsorption/photodegradation of dyes was fitted to pseudo-first-order

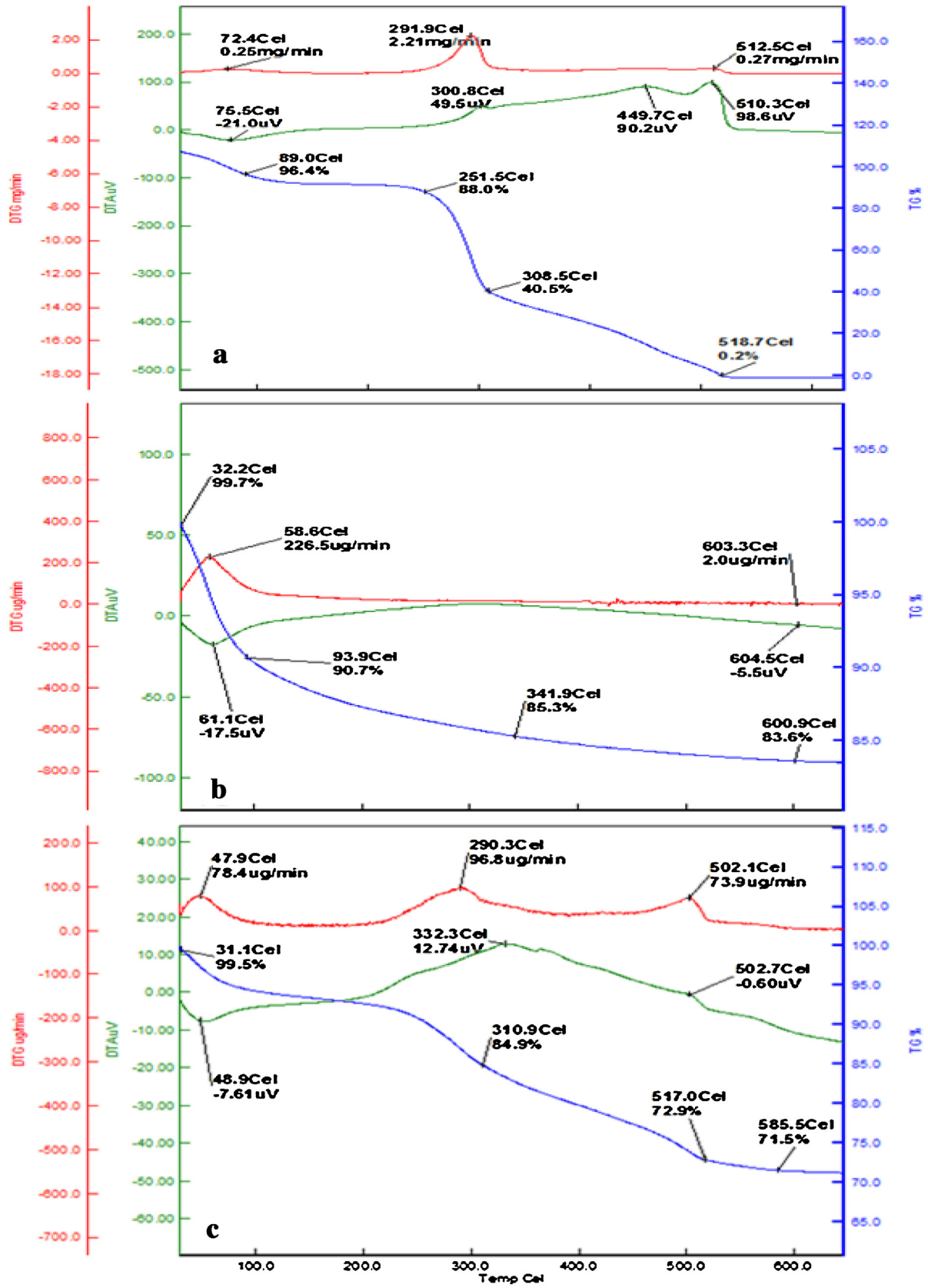

Fig. 6. TGA graphs of (a) GG (b) AO NPs and (c) GG/AO nanocomposite.

kinetics. The value of rate constant and regression coefficients (R^2) for MG is given in Table 1. The comparison of rate constants for coupled adsorption/photocatalysis and adsorption followed photocatalysis undoubtedly indicated that the photocatalysis under synergistic conditions was more proficient and effective.

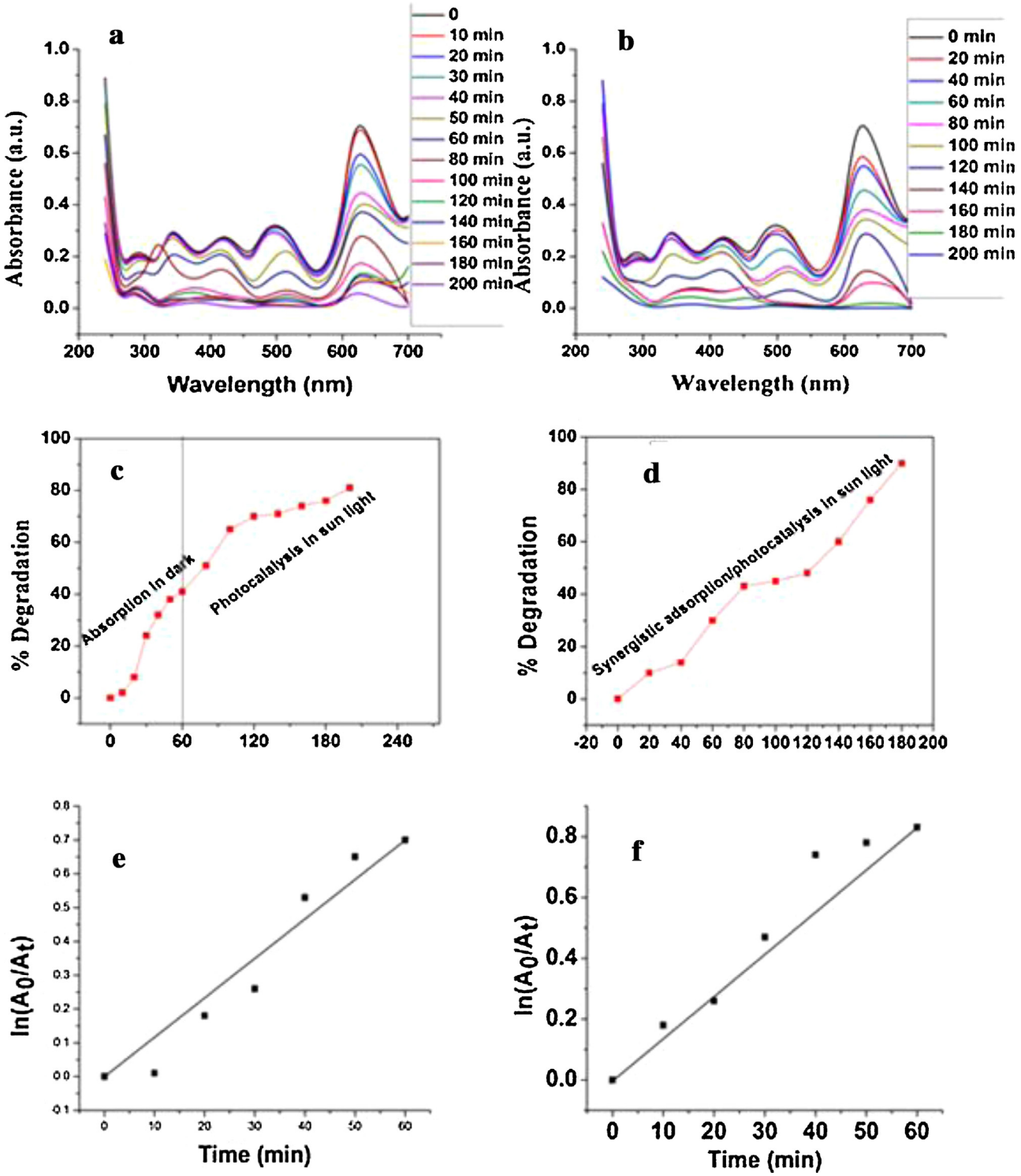

Fig. 7. Spectra of MG: (a) adsorption in dark followed by photocatalysis and (b) coupled adsorption/photocatalysis; percentage degradation of MG: (c) adsorption in dark followed by photocatalysis and (d) coupled adsorption/photocatalysis; pseudo-first-order kinetics for photodegradation of MG: (e) adsorption in dark followed by photocatalysis and (f) coupled adsorption/photocatalysis in presence of GG/AO nanocomposite (initial concentration of MG 1.5×10^{-5} M, pH-7, temperature -30 ± 5 °C).

The exceptional photodegradation performance of nanocomposite boosts its properties for waste water treatment.

3.4. Antibacterial activity

The antibacterial activity of prepared GG/AO nanocomposite was screened against *S. aureus*. It was observed that the GG/AO nanocomposite was capable to binding with the outer membrane of cell wall and preventing the nutrient transport inside the cell. The antibacterial effect was recorded more pronounced at high concentration of nanocomposite (Fig. 8). The antibacterial effect of nanocomposite might be due to the inhibition of dehydrogenase enzyme, periplasmic enzyme activity and active transport [52].

	0 hour	24 hours	48 hours
control	130000000	2.5E+17	8.7E+18
1 (0.4 μg/ml)	990000000	6.2E+12	9.5E+16
2 (0.8 μg/ml)	1250000000	2E+12	3.5E+14

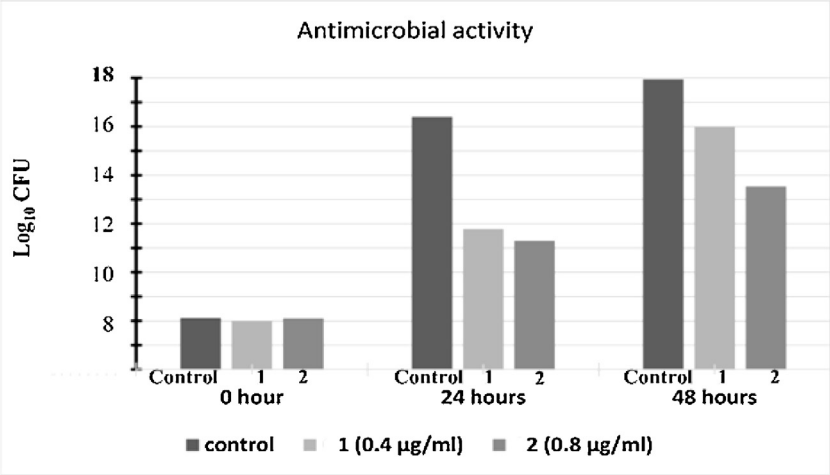

Fig. 8. Antibacterial efficiency of GG/AO nanocomposite against *S. aureus* bacteria.

4. Conclusion

The GG/AO nanocomposite was synthesized and characterized by different techniques to explore the functional group, bonding nature, crystallite nature, size and morphology. The TGA studies indicated high thermal stability of GG/AO as compared to AO. GG/AO nanocomposite showed the efficient photodegradation of MG dye. The coupled adsorption/photocatalysis was more efficient then adsorption followed by photocatalysis. The GG/AO nanocomposite showed a strong antibacterial activity against *S. aureus*.

Acknowledgments

The authors gratefully acknowledge the School of Chemistry, Shoolini University, India for providing the laboratory facilities. We also acknowledge to NIPER, Mohali, Punjab University, IIT Roorkee and Sultan Qaboos University for providing instrumental facilities for sample characterizations. The authors (M. Naushad & M.R. Khan) would like to extend their sincere appreciation to the Deanship of Scientific Research at King Saud University for funding this work through the Research Group No. RG-1437-004.

References

[1] (a) Z.A. Othman, M. Naushad, R. Ali, Kinetic, equilibrium isotherm and thermodynamic studies of Cr(VI) adsorption onto low cost adsorbent developed from peanut shell activated with phosphoric acid, Environ. Sci. Pollut. Res. 20 (2013) 3351–3365;
(b) A. Kumar, G. Sharma, M. Naushad, S. Thakur, SPION/β-cyclodextrin core–shell nanostructures for oil spill remediation and organic pollutant removal from waste water, Chem. Eng. J. 280 (2015) 175–187.

[2] X. Wu, J. Cai, S. Li, F. Zheng, Z. Lai, L. Zhu, T. Chen, Au@Cu_2O stellated polytope with core–shelled nanostructure for high-performance adsorption and visible-light-driven photodegradation of cationic and anionic dyes, J. Colloid Interface Sci. 469 (2016) 138–146.

[3] C.-G. Liu, T. Zheng, S. Liu, H.-Y. Zhang, Photodegradation of malachite green dye catalyzed by Keggin-type polyoxometalates under visible-light irradiation: transition metal substituted effects, J. Mol. Struct. 1110 (2016) 44–52.

[4] (a) H. Javadian, M.T. Angaji, M. Naushad, Synthesis and characterization of polyaniline–alumina nanocomposite: a comparative study for the adsorption of three different anionic dyes, J. Ind. Eng. Chem. 20 (2014) 3890–3900;
(b) M.R. Khan, M.A. Khan, Z.A. ALOthman, I.H. ALSohaimi, M. Naushad, N.H. ALShaalan, Quantitative determination of methylene blue in environmental samples by solid phase extraction and ultra performance liquid chromatography–tandem mass spectrometry: a green approach, RSC Adv. 4 (2014) 34037–34044.

[5] T. Robinson, G. McMullan, R. Marchant, P. Nigam, Remediation of dyes in textiles effluent: a critical review on current treatment technologies with a proposed alternative, Bioresour. Technol. 77 (2001) 247–255.

[6] N. Das, D. Charumathi, Remediation of synthetic dye from wastewater using—an overview, Indian J. Biotechnol. 11 (2012) 369–380.

[7] D. Pathania, G. Sharma, A. Kumar, Mu. Naushad, S. Kalia, A. Sharma, Z.A. ALOthman, Combined sorptional-photocatalytic remediation of dyes by polyaniline Zr(IV) selenotungstophosphate nanocomposite, Toxicol. Environ. Chem. 97 (2015) 526–537.

[8] R. Katwal, H. Kaur, G. Sharma, Mu. Naushad, D. Pathania, Electrochemical synthesized copper oxide nanoparticles for enhanced photocatalytic and antimicrobial activity, J. Ind. Eng. Chem. 31 (2015) 173–184.

[9] X. Wang, G. Liu, G.Q. Lu, H.M. Cheng, Stable photocatalytic hydrogen evolution from water over ZnO–CdS core–shell nanorods, Int. J. Hydrogen Energy 35 (2010) 8199–8205.

[10] A. Kumar, G. Sharma, M. Naushad, S. Thakur, SPION/β-cyclodextrin core–shell nanostructures for oil spill remediation and organic pollutant removal from waste water, Chem. Eng. J. 280 (2015) 175–187.

[11] A. Franco, M.C. Neves, M.M.L.R. Carrott, M.H. Mendonc, M.I. Pereira, O.C. Monteiro, Photocatalytic decolorization of methylene blue in the presence of TiO_2/ZnS nanocomposites, J. Hazard. Mater. 161 (2009) 545–550.

[12] (a) S.A. Nabi, Mu. Naushad, Studies of cation exchange thermodynamics for alkaline earths and transition metal ions on a new crystalline cation exchanger: aluminium tungstate and distribution coefficient values of metal ions in surfactant media, Colloid Surf. A: Phys. Eng. Aspects 293 (2007) 175–184;
(b) S.A. Nabi, Mu. Naushad, A.M. Khan, Sorption studies of metal ions on napthol blue–black modified amberlite IR-400 anion exchange resin. Separation and determination of metal ion contents of pharmaceutical preparation, Colloid Surf. A: Phys. Eng. Aspects 280 (2006) 66–70;
(c) Ahmed Shahat, Md. Rabiul Awual, Md. Abdul Khaleque, Md. Zahangir Alam, Mu. Naushad, A.M. Sarwaruddin Chowdhury, Large-pore diameter nano-adsorbent and its application for rapid lead(II) detection and removal from aqueous media, Chem. Eng. J. 273 (2015) 286–295.

[13] S. Srivastava, R. Sinha, D. Roy, Toxicological effects of malachite green, Aquat. Toxicol. 66 (2004) 319–329.

[14] F.P. Meyer, T.A. Jorgensen, Teratological and other effects of malachite green on the development of rainbow trout and rabbits, Trans. Am. Fish. Soc. 112 (1983) 818–824.

[15] V.K. Gupta, G. Sharma, D. Pathania, N.C. Kothiyal, Nanocomposite pectin Zr (IV) selenotungstophosphate for adsorptional/photocatalytic remediation of methylene blue and malachite green dyes from aqueous system, J. Ind. Eng. Chem. (2014) 957–964.

[16] D. Pathania, G. Sharma, M. Naushad, V. Priya, A biopolymer-based hybrid cation exchanger pectin cerium (IV) iodate: synthesis, characterization, and analytical applications, Desalt. Water Treat. 57 (2016) 468–475.

[17] G. Sharma, M. Naushad, D. Pathania, A. Mittal, G.E. El-desoky, Modification of *Hibiscus cannabinus* fiber by graft copolymerization: application for dye removal, Desalt. Water Treat. 54 (2015) 3114–3121.
[18] G. Robinson, S.B. Ross-Murphy, E.R. Morris, Viscosity-molecular weight relationships, intrinsic chains flexibility and dynamic solution properties of guar galactomannan, Carbohydr. Res. 107 (1982) 17–32.
[19] U. Smith, G. Holm, Effect of a modified guar gum preparation on glucose and lipid levels in diabetics and healthy volunteers, Atherosclerosis 43 (1982) 1–10.
[20] H.M. Wang, D. Liang, F.F. Han, G.Q. Tang, X.C. Xu, Structure and conducting mechanism of polythiophene/multi-walled carbon nanotube composites, Acta. Chim. Sin. 66 (2008) 2279–2284.
[21] M. Lanzi, L. Paganin, New regioregular polythiophenes functionalized with sulfur-containing substituents for bulk heterojunction solar cells, React. Funct. Polym. 70 (2010) 346–360.
[22] X.Z. Guo, Y.F. Kang, T.L. Yang, S.R. Wang, Low-temperature NO_2 sensors based on polythiophene/WO_3 organic-inorganic hybrids, Trans. Nonferrous Met. Soc. China 22 (2012) 380–385.
[23] R. Jayakumar, R. Ramachandran, V.V. Divyarani, K.P. Chennazhi, H. Tamura, S.V. Nair, Fabrication of chitin–chitosan/nano TiO_2-composite scaffolds for tissue engineering applications, Inter. J. Biol. Macromol. 48 (2011) 336–344.
[24] D. Gupta, D. Singh, N.C. Kothiyal, A.K. Saini, V.P. Singh, D. Pathania, Synthesis of chitosan-*g*-poly (acrylamide)/ZnS nanocomposite for controlled drug delivery and antimicrobial activity, Inter. J. Biol. Macromol. 74 (2015) 547–557.
[25] G. Sharma, D. Pathania, M. Naushad, Preparation, characterization and antimicrobial activity of biopolymer based nanocomposite ion exchanger pectin zirconium (IV) selenotungstophosphate: Application for removal of toxic metals, J. Ind. Eng. Chem. 20 (2014) 4482–4490.
[26] V. Singh, P. Kumari, S. Pandey, T. Narayan, Removal of chromium(VI) using poly (methylacrylate) functionalized guar gum, Bioresour. Technol. 100 (2009) 1977–1982.
[27] V. Singh, S. Pandey, S.K. Singh, R. Sanghi, Removal of cadmium from aqueous solutions by adsorption using poly(acrylamide) modified guar gum–silica nanocomposites, Sep. Purif. Technol. 67 (2009) 251–261.
[28] L. Yan, P.R. Chang, P. Zheng, X. Ma, Characterization of magnetic guar gum–grafted nanotube and the adsorption of the dyes, Carbohydr. Polym. 87 (2012) 1919–1924.
[29] S. Kureti, W. Weisweiler, A new route for the synthesis of high surface area γ-aluminium oxide xerogel, Appl. Catal. A Gen. 225 (2002) 251.
[30] T. E. Cottringer, H. Ronald, Abrasive matrial and method for preparing the same, United States Patent, Patent no. 4, 623, 364; Patent date. November 18, 1986.
[31] L. Onnby, C. Svensson, L. Mbundi, R. Busquets, A. Cundy, H. Kirsebom, γ-Al_2O_3-based nanocomposite adsorbents for arsenic(V) removal: assessing performance, toxicity and particle leakage, Sci. Total Environ. 473–474 (2014) 207–214.
[32] L. Onnby, V. Pakade, B. Mattiasson, H. Kirsebom, Polymer composite adsorbents using particles of molecularly imprinted polymers or aluminium oxide nanoparticles for treatment of arsenic contaminated waters, Water Res. 46 (2012) 4111–4120.
[33] N.B. Abaffy, D.G. McCulloch, J.G. Partridge, Aluminium/aluminium oxide nanocomposites prepared using a filtered cathodic vacuum arc, Surf. Coat. Techol. 207 (2012) 529–534.
[34] R.K. Goyal, Y.S. Negi, A.N. Tiwari, High performance polymer composites on PEEK reinforced with aluminum oxide, J. Appl. Polym. Sci. 100 (2006) 4623–4631.
[35] D. Pathania, G. Sharma, Mu. Naushad, A. Kumar, Synthesis and characterization of a new nanocomposite cation exchanger polyacrylamide Ce (IV) silicophosphate: photocatalytic and antimicrobial applications, J. Ind. Eng. Chem. 20 (2014) 3596–3603.
[36] G. Sharma, Amit Kumar, M. Naushad, M.R. Khan, Lanthanum/cadmium/polyaniline bimetallic nanocomposite for the photodegradation of organic pollutant, Iran. Polym. J. 24 (2015) 1003–1013.
[37] A. Mittal, V.K. Gupta, A. Malviya, J. Mittal, Adsorption of hazardous dye crystal violet from wastewater by waste materials, J. Hazard Mater. 151 (2008) 821–832.
[38] C.W. Lin, B.J. Hwang, C.R. Lee, Methanol sensors based on the conductive polymer composites from polypyrrole and poly(vinyl al- cohol), Mater. Chem. Phys. 55 (1998) 139–144.
[39] D. Pathania, G. Sharma, A. Kumar, N.C. Kothiyal, Fabrication of nanocomposite polyaniline zirconium (IV) silicophosphate for photocatalytic and antimicrobial activity, J. Alloy Comp. 588 (2014) 668–675.
[40] S. Pal, Y.K. Tak, J.M. Song, Does the antibacterial activity of silver nanoparticles depend on the shape of the nanoparticle? a study of the gram-negative bacterium *Escherichia coli*, Appl. Environ. Microbiol. (2007) 1712–1720.
[41] D. Pathania, G. Sharma, R. Thakur, Pectin@ zirconium (IV) silicophosphate nanocomposite ion exchanger: Photo catalysis, heavy metal separation and antibacterial activity, Chem. Eng. J. 267 (2015) 235–244.
[42] J. Gangwara, K.K. Dey, Komal, Praveen, S.K. Tripathib, A.K. Srivastavaa, Microstructure, phase formations and optical bands in nanostructured alumina, Adv, Mat. Lett. 2 (2011) 402–408.
[43] H. Chang, Y.C. Chang, Fabrication of Al_2O_3 nanofluid by a plasma arc nanoparticles synthesis system, J. Mater. Proc. Technol. 207 (2008) 193–199.
[44] V.S. Kortov, S.V. Nikiforov, I.I. Milman, E.V. Moiseykin, Specific features of luminescence of radiation-colored α-Al_2O_3 single crystals, Radiat. Meas. 38 (2004) 451–454.
[45] F. Li, J. Wu, Q. Qin, Z. Li, X. Huang, Optical and photocatalytic properties of novel CuS nanoplate-nased architectutes synthesized by solvothermal rout, Crystal Res. Technol. 44 (2009) 729–735.
[46] T.A. Khan, M. Nazir, I. Ali, A. Kumar, Removal of chromium(VI) from aqueous solution using guar gum–nano zinc oxide biocomposite adsorbent, Arab. J. Chem. (2013), http://dx.doi.org/10.1016/j.arabjc.2013.08.019.
[47] B.N. Kim, K. Hiraga, K. Morita, H. Yoshida, T. Miyazaki, Y. Kagawa, Microstructure and optical properties of transparent alumina, Acta Mater. 57 (2009) 1319–1326.
[48] S.S. Prasad, K.M. Rao, P.R.S. Reddy, N.S. Reddy, K.S.V. Krishna Rao, M.C.S. Subha, Synthesis and Characterisation of guar gum-*g*-poly(acrylamidoglycolic acid) by redox initiator, Indian J. Adv. Chem. Sci. 1 (2012) 28–32.
[49] B. Sathyaseelan, I. Baskaran, K. Sivakumar, Phase transition behavior of nanocrystalline Al_2O_3 Powders, Soft Nanosci. Lett. 3 (2013) 69–74.
[50] A. Kumar, G. Sharma, Mu. Naushad, P. Singh, S. Kalia, Polyacrylamide/$Ni_{0.02}Zn_{0.98}O$ nanocomposite with high solar light photocatalytic activity and efficient adsorption capacity for Toxic Dye Removal, Ind. Eng. Chem. Res. 53 (2014) 15549–15560.
[51] W. Ueda, M. Sadakane, H. Ogihara, Nano-structuring of complex metal oxides for catalytic oxidation, Catal. Today 132 (2008) 2–8.
[52] G.M. Mansour, E. Hassan, Synthesis characterization and antibacterial properties of a novel nanocomposite based on polyaniline/polyvinyl alcohol/Ag, Arab. J. Chem. 7 (2014) 846–855.